ARTICLES

Ultrafast Studies of Photoexcited Electron Dynamics in γ- and α-Fe_2O_3 Semiconductor Nanoparticles

Nerine J. Cherepy,[†] Dorion B. Liston,[†] Jennifer A. Lovejoy,[†] Hongmei Deng,[‡] and Jin Z. Zhang*,[†]

Department of Chemistry, University of California, Santa Cruz, Santa Cruz, California 95064, and Research Center for Analysis and Measurement, Fudan University, Shanghai, 200433, China

Received: September 29, 1997; In Final Form: November 19, 1997

The ultrafast dynamics of photoexcited electrons in the semiconductor iron oxides, γ-Fe_2O_3 and α-Fe_2O_3, have been measured using femtosecond laser spectroscopy. Transmission electron microscopy shows the γ-Fe_2O_3 particles are spherical, with 1−2 nm average diameter, and the α-Fe_2O_3 are spindle-shaped, with average dimensions of 1×5 nm. Static electronic absorption measurements of the colloids suggest that they may be in the quantum confined regime. Steady-state emission measurements show that the <400 nm direct transitions are moderately emissive, but the indirect transitions in the visible do not produce measurable emission. The ultrafast transient absorption decay profiles measured for the γ-Fe_2O_3 and α-Fe_2O_3 samples synthesized in our lab as well as a commercial sample of γ-Fe_2O_3 are the same and are fit best with three exponentials with 0.36, 4.2, and 67 ps time constants. The decay profiles are independent of pump power, probe wavelength, and pH and were not affected by lattice doping with other metals or surface adsorbates for the cases studied. This fast overall decay, in conjunction with very weak fluorescence, suggests extremely efficient nonradiative relaxation, possibly related to the dense band structure, a high density of trap states, or simply strong coupling between trap states. The fast relaxation of photoexcited electrons in the conduction band and trap states is consistent with the low photocurrent efficiency of typical Fe_2O_3 electrodes.

Introduction

Iron oxides are technologically useful as pigments and semiconductors and for their magnetic properties.[1] The stability and semiconductor properties of α-Fe_2O_3 allow it to be used as a photocatalyst,[2−8] while the magnetic properties of γ-Fe_2O_3[9−13] make it a common active component of high-density recording media. Despite numerous investigations, the semiconductor and optical properties of the iron oxides have not been well characterized, and there have been no studies reported on their ultrafast charge carrier dynamics. A better understanding of their optical properties and excited carrier dynamics will be invaluable in developing applications of iron oxide nanoparticles in photocatalysis and, possibly, in magnetooptical devices.

The two forms of Fe_2O_3 differ in many aspects. The unit cell of γ-Fe_2O_3 is cubic, with both octahedrally and tetrahedrally coordinated Fe^{3+} sites (defect spinel structure), while α-Fe_2O_3 has a hexagonal unit cell and entirely octahedrally coordinated Fe^{3+} atoms (corundum structure).[1] The γ-Fe_2O_3 particles studied here are spherical, while the α-Fe_2O_3 particles are spindle-shaped. Bulk γ-Fe_2O_3 is ferrimagnetic, while, in contrast, bulk α-Fe_2O_3 is classified as either weakly ferromagnetic or antiferromagnetic.[1] However, both γ-Fe_2O_3 and α-Fe_2O_3 nanoparticles smaller than ∼10 nm are superparamagnetic since they are smaller than a single magnetic domain.[1,14−19] The electronic structure of the iron oxides consists of Fe^{3+} ligand field transitions and excitations involving coupled adjacent Fe^{3+} cations in the visible and near-UV range and ligand-to-metal charge-transfer transitions in the UV.[1,20]

The strong absorptivity of Fe_2O_3 in the visible range, along with its abundance and low cost, has stimulated considerable interest in its use as a photocatalyst and a photoelectrode. However, conductivity and photocurrent quantum efficiency of both forms of Fe_2O_3 are low.[3,21−29] Although the bandgap of α-Fe_2O_3 is 2.2 eV (564 nm), the visible transitions are thought to be indirect transitions (d → d type)[20,24,30] and are not strongly absorptive. Direct transitions from 2p O^{2-} valence band orbitals to the conduction band edge occur at 3−4.7 eV (257−413 nm).[20,24,30] Photocurrent quantum efficiency, even for an optimized zinc-doped iron oxide electrode, is only 0.8% at the maximum of the photocurrent spectrum.[28] Generally, α-Fe_2O_3 has a resistivity of 10^3-10^6 Ω·cm, decreasing for samples doped with other metal ions.[27−29] However, a Mg-doped iron oxide electrode with a resistivity of $10-10^2$ Ω·cm has been reported.[31] In general, recombination of electrons and holes, trapping of electrons by oxygen-deficient iron sites, and low mobilities of holes are considered to be responsible for the low conductivities and poor photocurrent efficiencies of iron oxide electrodes.[24,27,31]

Correlation of quantum efficiency of a nanocrystalline electrode with photoexcited electron dynamics of the corresponding nanoparticle can reveal the contribution of the initial decay kinetics to the overall quantum efficiency of the electrode. Thus, the identification of materials that have an intrinsically

* Corresponding author.
[†] University of California, Santa Cruz.
[‡] Fudan University.

S1089-5647(97)03149-0 CCC: $15.00
Published on Web 01/13/1998

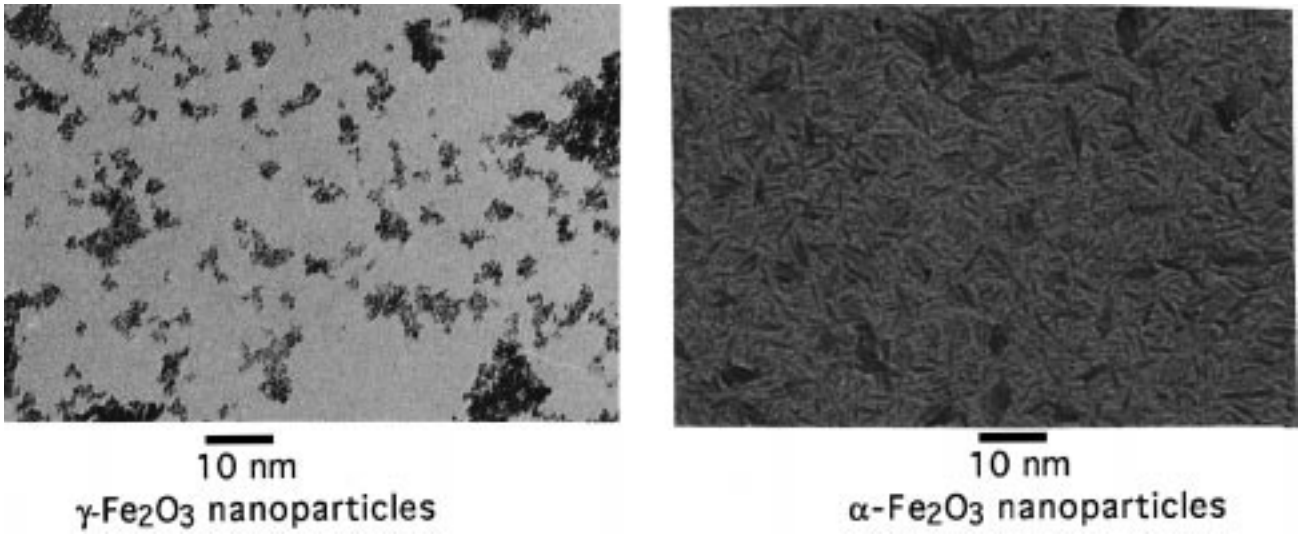

Figure 1. TEM photographs of the samples synthesized in our lab and used in this study: (A, left) γ-Fe_2O_3 (maghemite) and (B, right) α-Fe_2O_3 (hematite).

slow decay of photoexcited electrons would help in the search for high-efficiency photocatalysts and photoelectrodes. Here, we provide an initial kinetic study of photoexcited charge carriers in γ-Fe_2O_3 and α-Fe_2O_3 nanoparticles. The results show that the photoexcited electrons are overall very short-lived and the decay is primarily nonradiative. A power-dependence study reveals that the relaxation mechanism for the early time decay is very different from that found in other semiconductor nanoparticles, e.g., CdS[32] or TiO_2.[33]

Experiment

Many studies detailing the synthesis of γ-Fe_2O_3 and α-Fe_2O_3 nanoparticles have been reported.[5,7,9,13,16,34−36] Nanoparticles of γ-Fe_2O_3 were prepared by the selective reaction and oxidation of Fe^{2+} and Fe^{3+}. An ionic solution was prepared by adding 0.52 g of $FeCl_3$ and 0.2 g of $FeCl_2$ to 20 mL of Milli-Q H_2O. The resulting solution was added dropwise to 25 mL of 1.0 M NaOH.[9] A black precipitate of Fe_3O_4 was produced instantly, the particles of which aggregate readily in the presence of a magnetic field. Then, γ-Fe_2O_3 was prepared by acidification of the Fe_3O_4 solution to pH = 3.5 with HCl and subsequent aeration at 25 °C with ambient air (30 mL/min). The solution changed from black to a muddy, chocolate brown after 30 min of aeration. This solution was centrifuged and the supernatant reserved. To prepare doped γ-Fe_2O_3 particles, 10 mol % metal (Zn, Co, Cr, or Cu) chloride salt was added to the solution of iron chlorides before addition of NaOH, and the preparation was carried out as for the undoped colloid. For studies involving adsorbates, Acid Orange II or deoxykenocholic acid was adsorbed onto γ-Fe_2O_3 from 10^{-3} M solutions (ratio of adsorbate molecules/particle was ∼50−100). Spherical particles of ∼2 nm diameter have surface areas of ∼12 nm^2, and therefore under these conditions there is clearly an excess of adsorbates to surface defects. Commercial γ-Fe_2O_3 was obtained from Alfa, suspended in deionized water, sonicated, and centrifuged, and the supernatant was reserved. Colloidal particles of α-Fe_2O_3 were prepared by adding a 32% solution of $FeCl_3$ (1.2 mL) to 75 mL of boiling Milli-Q water. The resulting reddish-brown sol was centrifuged, and the supernatant was decanted and stored. All the colloidal sols were diluted to yield an OD = 1 at 390 nm for laser experiments or diluted to OD = 0.15 for fluorescence measurements.

The TEM measurements were acquired with a JEOL-100 CX transmission electron microscope with 20 000× magnification. UV−visible absorption spectra were taken with a Hewlett-Packard 8452A diode array spectrophotometer and referenced to water. Fluorescence spectra were recorded on a Jobin Yvon-Spex Fluoromax 2 spectrofluorimeter. The electron decay dynamics were measured using a pump−probe scheme with a regeneratively amplified, mode-locked Ti−sapphire laser. The laser system and the experimental setup have been previously described.[37] Pulses of 40 fs duration and 5 nJ/pulse were generated from a Ti−sapphire oscillator pumped with an Ar^+ laser (Coherent) and then amplified in a regenerative amplifier (Quantronix) using chirped-pulse amplification. The final output was 150 fs pulses with 250 μJ/pulse centered at 780 nm and at 1 kHz. The output was passed through a KDP crystal to generate 390 nm light at 30 μJ/pulse, which was attenuated with neutral density filters and used to excite the sample. The remaining beam was focused into a quartz flat with a 1 cm optical path length to generate white light from which a probe pulse, e.g. 720 nm, was selected using band-pass filters (fwhm 10 nm). The time delay between the excitation beam and the probe beam was controlled by a translation stage with 1 μm resolution. The transient absorption decays were fit with a nonlinear least-squares algorithm and Igor Pro software.

Results

Using transmission electron microscopy, the colloidal particles of Fe_3O_4 (precursor to γ-Fe_2O_3 particles) were found to be spherical with diameter ∼1 nm (not shown). The particles of γ-Fe_2O_3 were also spherical and uniform in size with diameters of 1−2 nm (Figure 1A). The electron micrograph of the α-Fe_2O_3 particles (Figure 1B) reveals very distinct nanocrystals with well-defined facets of mean dimensions 1 × 5 nm in a spindle shape. The sample prepared with the γ-Fe_2O_3 particles supplied by Alfa had a broader size distribution, centered at ∼50 nm.

The electronic absorption spectra of the iron oxides are shown in Figure 2, along with their emission spectra. The semiconductors exhibit a broad absorption in the visible region, extending into the UV, with bands at ∼200, ∼230, ∼285, and ∼340 nm for α-Fe_2O_3 and a tail extending to ∼560 nm while only the bands at ∼200 and ∼285 nm are clearly observed for γ-Fe_2O_3. Emissions of these semiconductors excited at 300 nm

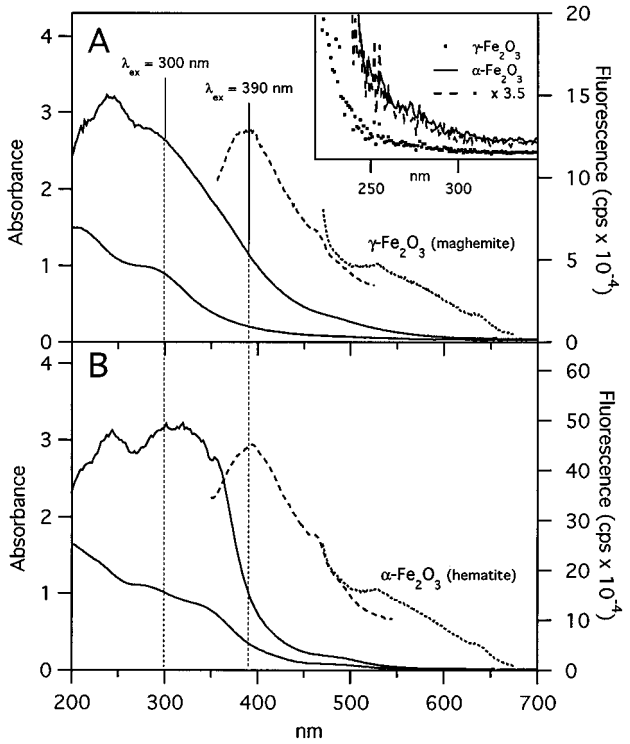

Figure 2. Absorption (—) and emission spectra excited at 300 nm (---) and excited at 390 nm (•••) of (A) γ-Fe_2O_3 (maghemite) and (B) α-Fe_2O_3 (hematite). The pump wavelength of 390 nm used in the ultrafast measurements is also shown. Two absorption spectra are shown for each sample; the samples with OD $\sim$ 1 were used in the pump−probe experiments, while the spectra for the dilute samples are used to show the absorption line shape. The inset shows the excitation spectrum for emission detected at 400 nm.

(dashed line) and 390 nm (dotted line) are also shown in Figure 2. The emission spectra for the two samples are about the same, except that the α-Fe_2O_3 emission is about 4 times more intense. An excitation profile, shown as an inset in Figure 2, of the emission at 400 nm for both samples shows greatly enhanced emission with excitation <250 nm. The emission yield for the γ-Fe_2O_3 particles excited at 390 nm is $\sim 1 \times 10^{-5}$.

The ultrafast transient absorption profile of γ-Fe_2O_3 is shown on three different time scales in Figure 3. A pulse-width limited rise of the signal is followed by a decay that can only be fit to a multiple exponential. A very good fit (solid lines) may be obtained using three exponentials with 0.36, 4.2, and 67 ps time constants convolved with a Gaussian (fwhm 200 fs) representing the cross-correlation of the pump and probe pulses. The transient absorption decays of γ-Fe_2O_3, α-Fe_2O_3, and the commercial γ-Fe_2O_3 sample are compared on the 0−8.3 ps time scale in Figure 4A. The 0−43 ps window is shown for the γ-Fe_2O_3 and α-Fe_2O_3 samples in Figure 4B. In all cases the decay profiles overlay perfectly and can be fit with the same time constants.

The decay dynamics for γ-Fe_2O_3 nanoparticles were found to be linear with pump power, as shown in Figure 5. The power was varied between 0.4 and 1.2 mJ/(pulse cm^2), with no change in the time constants or the relative amplitudes of the different decay components. There also appears to be little, if any, wavelength dependence of the transient absorption decay profiles probed between 660 and 850 nm, as shown in Figure 6.

The effects of surface-adsorbed molecules on the dynamics of the excited electrons in Fe_2O_3 were studied as well. Deoxykenocholic acid, known to adsorb well to TiO_2,[38] was adsorbed onto Fe_2O_3 colloid. Another sample was prepared with

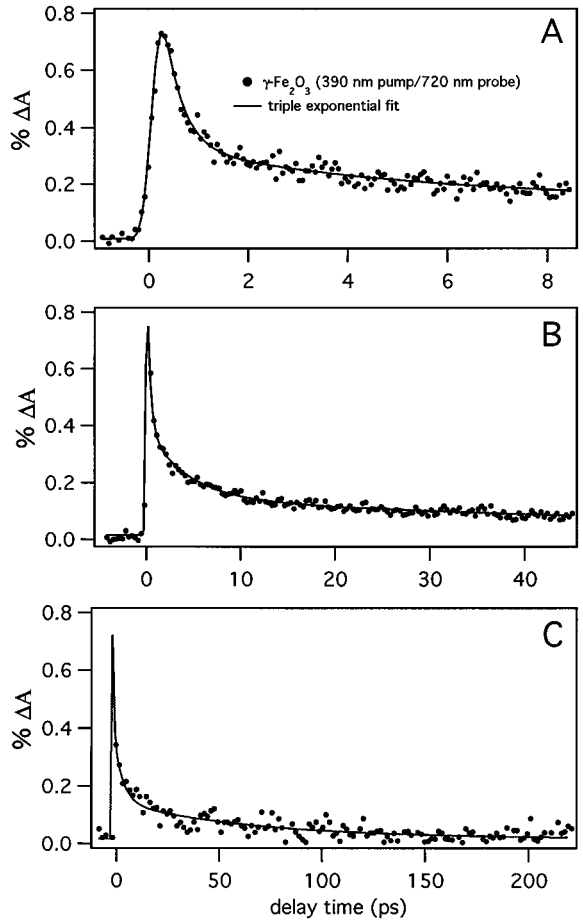

Figure 3. Ultrafast transient absorption decay profiles of γ-Fe_2O_3 nanoparticles. (A) The 0−8.3 ps, (B) the 0−48 ps, and (C) the 0−230 ps windows are fit simultaneously using a nonlinear least-squares fitting algorithm to a triple-exponential decay convolved with a Gaussian representing the cross-correlation of the 390 nm pump (1.2 mJ/(pulse cm^2)) and 720 nm probe pulses. The transient absorption has a pulse-width limited rise time and is best fit to a triple exponential with 0.36, 4.2, and 67 ps time constants (solid line).

the azo dye Orange II as a surface-adsorbed species. This dye is known to degrade in the presence of light and oxygen on TiO_2[39] and with the photo-Fenton reagent (Fe^{3+} and H_2O_2).[40] Studies of photochemical surface reactions, such as the degradation of Orange II, should help determine the usefulness of Fe_2O_3 nanoparticles in photocatalysis. The ultrafast transient absorption profiles (not shown) of these two adsorbate-capped samples of Fe_2O_3 do not differ from those of the bare Fe_2O_3 colloid. Thus, Orange II does not appear to react with the electron or hole photogenerated in Fe_2O_3 on the time scale studied (<600 ps). However, a signal corresponding to such reaction on a longer time scale is possible but beyond the capability of our current instrument. It should be pointed out that this study only indicates that the surface adsorbate, Orange II, does not seem to influence noticeably the electron dynamics; it cannot rule out completely that the surface defects are important.

To further investigate the role of surface species on the transient absorption decay of Fe_2O_3 colloids in aqueous solution, pH was varied between 3 and 6, but the ultrafast transient absorption profile was still unaffected. At pH lower than 3 the colloids dissolved, and at pH higher than 6 they aggregated. The ultrafast transient absorption was also measured for γ-Fe_2O_3 doped with 10% (moles of dopant/moles of Fe) Zn, Co, Cr, or Cu. The decay profile was also unchanged in the doped γ-Fe_2O_3 samples.

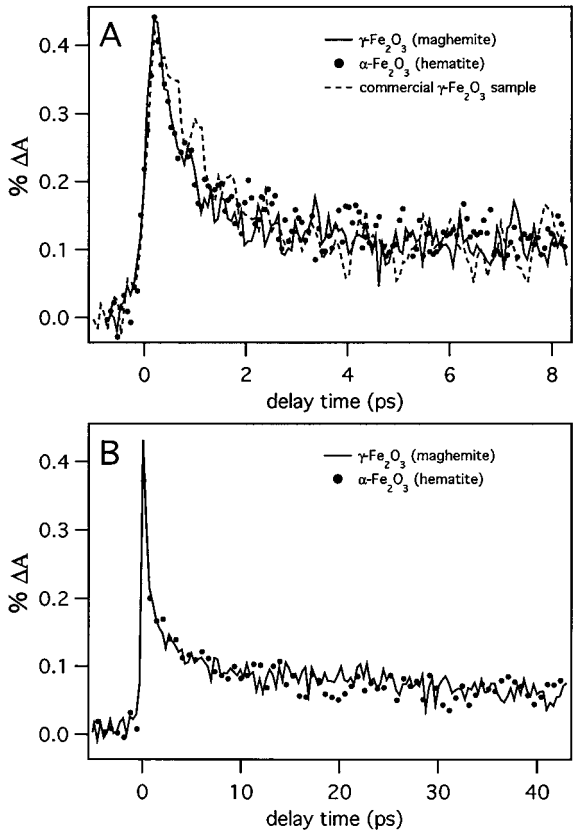

Figure 4. Transient absorption decay profiles of nanoparticles of γ-Fe_2O_3 (average diameter 1−2 nm), α-Fe_2O_3 (average dimensions 1 × 5 nm) synthesized in our lab, and a commercial sample of γ-Fe_2O_3 (broad particle size distribution, centered at ∼50 nm) on two different time scales and acquired with 390 nm pump (0.6 mJ/(pulse cm^2)) and 720 nm probe.

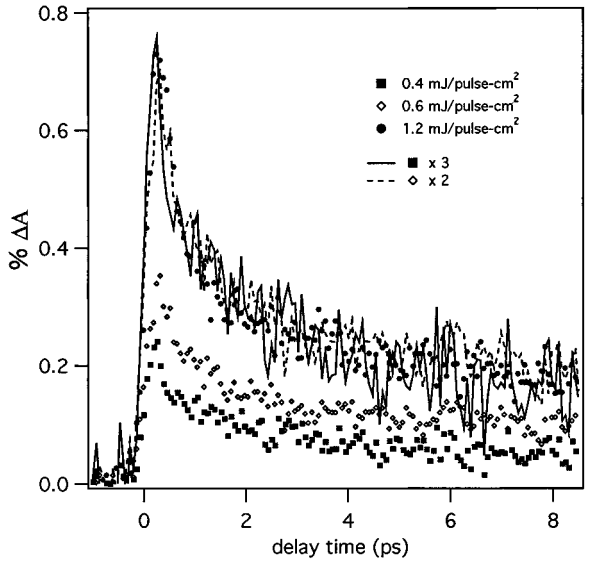

Figure 5. Transient absorption decay profiles of γ-Fe_2O_3 acquired with 390 nm pump and 720 nm probe at different pump powers: 0.4 mJ/(pulse cm^2) (closed squares), 0.6 mJ/(pulse cm^2) (open diamonds), and 1.2 mJ/(pulse cm^2) (closed circles). The scaled 0.4 mJ/(pulse cm^2) trace (solid line) and the scaled 0.6 mJ/(pulse cm^2) trace (dashed line) agree well with the 1.2 mJ/(pulse cm^2) trace, indicating no change in the time constants and relative amplitudes of different decay components with increasing power.

Discussion

Static Optical Absorption and Emission. Since the accepted bandgap energies for bulk γ-Fe_2O_3 and α-Fe_2O_3 are 611 and 564 nm, respectively, it is somewhat surprising to detect emission at above bandgap energy. The visible tails of the absorption spectra of the colloids studied here are somewhat blue-shifted from these values and in agreement with earlier reports that the absorption edge shifts with decreasing nanoparticle size for α-Fe_2O_3 particles in the 1−60 nm range.[7] No literature value for the exciton radius of Fe_2O_3 could be found, although many measurements of the onset of superparamagnetic behavior for particles of both γ-Fe_2O_3 and α-Fe_2O_3 with diameters <10 nm[1,14−19] support the conclusion that the particles studied here may be in the quantum-confined regime. However, the emission band measured at higher energy than the bandgap is probably due to the intrinsic properties of the electronic transitions in iron oxides, not quantum confinement. Most likely, the ∼400 nm emission band originates with the ligand-to-metal charge-transfer transitions (thought to be direct transitions), while the Fe^{3+} ligand field and Fe^{3+}−Fe^{3+} pair transitions (indirect transitions) extending into the visible produce no measurable emission.[1,20] The excitation profile of the 400 nm emission, shown in the inset in Figure 2A, has an onset at ∼250 nm, in good agreement with the first ligand-to-metal charge-transfer transition, calculated at 250 nm for γ-Fe_2O_3 and 270 nm for α-Fe_2O_3.[20] It has been noted that the fluorescence yield at 390 nm excitation is very low, $\sim 10^{-5}$, indicating that most of the photogenerated electrons at 390 nm decay nonradiatively. This is consistent with the very short electron lifetime observed in the transient absorption measurements.

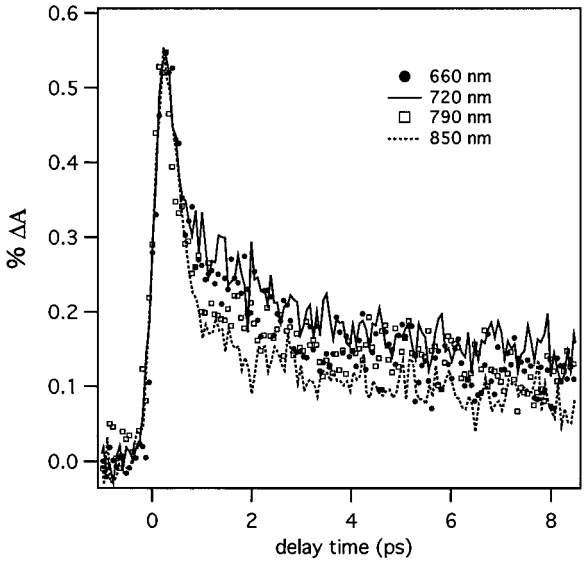

Figure 6. Wavelength dependence of the dynamics of γ-Fe_2O_3 nanoparticles. Rise time (pulse-width limited) and decay kinetics for traces acquired with 660 nm (closed circles), 720 nm (solid line), 790 nm (open squares), and 850 nm probe (dotted line) are in good agreement.

Assignment of Transient Absorption Signal. Before discussing the possible decay mechanisms of the photogenerated electrons, we will comment on the assignment of the observed transient absorption signal in the red to near-IR region. Red to near-IR transient absorption of photoexcited electrons has been observed before in metal oxide semiconductor nanoparticles, such as TiO_2[33] and ZnO,[41] and the signal has been assigned to trapped electrons following rapid trapping (<150 fs) from the conduction band. In principle, the transient absorption in this spectral region could have contributions from electrons both in the conduction band and in trap states. Upon excitation with greater than bandgap energy, the electrons are created as "hot" carriers which rapidly (<100 fs) thermalize and relax to the

bottom of the conduction band. Since hot electrons are expected to be very short-lived and have absorption mostly in the IR region, their contribution to the observed signal in the red to near-IR region is expected to be insignificant. Thermalized electrons at the bottom of the conduction band and excitons (bound electron−hole pairs), which usually lie slightly below the bottom of the conduction band, may have significant absorption in this spectral region and thus contribute to the observed transient absorption.[42] The thermalized electrons in the conduction band may recombine directly with holes in the valence band and trap states, or they may relax via intrinsic lower-lying electronic states, if present, and defect trap states, from which they further decay by radiative and nonradiative pathways. The nonradiative pathways are usually found to dominate for colloidal semiconductor nanoparticles with a high density of trap states.

For Fe_2O_3 there are several low-lying electronic states (bands) below the bottom of the band reached by the 390 nm photon.[20] These states, which will be referred to as mid-bandgap states, provide additional relaxation pathways for the initially photogenerated electrons, which are energetically similar to trap states created by surface or internal defects of the particles. This makes it somewhat difficult to distinguish the relative contribution or influence that these intrinsic mid-bandgap states have, versus trap states, on the relaxation process, as discussed in more detail later.

Lack of wavelength dependence of the transient absorption decay profile, apparent in Figure 6, indicates a broad absorption spectrum for the photoexcited electrons. This lack of dependence of the dynamics on probe wavelength may be interpreted as showing that the carriers are thermalized within the laser pulse (∼150 fs), since no spectral shift can be correlated with cooling. A previous study of the absorption spectrum of electrons injected into α-Fe_2O_3 particles through pulse radiolysis assigned a broad absorption band extending at least from 500 to 900 nm to electrons trapped at Fe^{3+} sites, reducing them to Fe^{2+}.[42] No evidence of free conduction band electron absorption was observed. This is in contrast to TiO_2 particles for which a broad absorption extending through the infrared region was identified as due to free electrons in the conduction band while trapped electrons were found to have a relatively narrow absorption band with a peak in the visible to red region.[42] If one could monitor the electrons relaxing from the conduction band to more localized trap states in time, a narrowing and blue shift of the electron absorption spectrum would be expected. When measurements are performed with a single probe wavelength at a time, as in the present study, a faster relaxation time should be expected for redder probe wavelengths than for blue wavelengths, similar to the wavelength dependence observed in vibrational relaxation in many molecules in liquids. Thus, the lack of a probe wavelength dependence of the decay times for Fe_2O_3 observed here seems to suggest that the decays are not due to trapping and that the transient absorption signal in the red−near-IR is dominated by trapped electrons and/or mid-bandgap states. If there is any contribution from thermalized conduction band electrons or, possibly, excitons (especially at early times), this contribution is small. This suggestion is consistent with earlier studies which indicated that electron trapping is predominant in Fe_2O_3 nanoparticles.[42]

Transient Absorption Decays: Mechanisms of Photoexcited Electron Relaxation. A number of reports of ultrafast electron dynamics in semiconductor nanoparticles provide some benchmarks with which to compare the kinetics of photoexcited electrons in Fe_2O_3. The decay of near-IR transient absorption of photoexcited electrons has been previously reported for TiO_2,[33] ZnO,[41] CdS,[32,37] CdZnS,[32] CdSe,[32] and AgI.[43] Ideally, certain decay pathways could be identified and assigned as universal electron relaxation mechanisms, or possibly different systems could be used to test the limits of a single model. For TiO_2, ZnO, CdS, and CdSe at low excitation intensities, a tens of picoseconds transient absorption decay may be assigned to the trapping of conduction band electrons, while a long-lived transient absorption (>0.5 ns) is due to trapped electrons.[32] At higher excitation powers, the amplitude of a fast (1−5 ps) decay component increases nonlinearly with excitation intensity, and its time constant decreases with increasing intensity. The mechanism for this decay has been proposed to be exciton−exciton annihilation.[32] In contrast, photoexcited AgI nanoparticles show a two-component, power-independent profile, with a 2.5 ps decay and a >0.5 ns component. The >0.5 ns decay was assigned to reaction of deep trapped electrons with interstitial silver ions to form silver metal clusters, while the fast component was attributed to trapping or fast electron−hole recombination mediated by a high density of trap states.[43]

Similar to AgI, the transient absorption decay profiles measured here for γ-Fe_2O_3 and α-Fe_2O_3 are independent of power. However, no significant transient absorption component remains beyond 100 ps for Fe_2O_3, which is in contrast to AgI which exhibits a long-lived (>0.5 ns) component. The decay for Fe_2O_3 (70% of the transient absorption disappears within 8 ps) is much faster than any of the semiconductors studied thus far,[32,33,41,43] and furthermore, it is completely independent of excitation intensity (see Figure 5). Since the lack of dependence of the decay profile on excitation power is similar to AgI but in contrast with TiO_2, ZnO, CdS, and CdSe, the exciton−exciton annihilation decay mechanism does not seem to be in operation for AgI or Fe_2O_3, at least not within the excitation power regime studied here. The lack of a long-lived transient absorption component for Fe_2O_3, as observed for TiO_2, ZnO, CdS, CdSe, and AgI, suggests that no trapped carriers remain in Fe_2O_3 beyond 100 ps.

The decay mechanisms of photoexcited charge carriers in Fe_2O_3 nanoparticles therefore appear to be different from those of the semiconductors which exhibit strong power dependence of their fast decay components. Since the power-dependent decay attributed to exciton−exciton annihilation is thought to arise upon trap saturation,[32] this suggests that alternative relaxation mechanisms or additional relaxation pathways are responsible for the decays observed in Fe_2O_3.

If the transient absorption signal is dominated by thermalized conduction band electrons (and excitons or shallow trapped electrons at thermal equilibrium with the conduction band), the decays observed can be attributed to trapping, relaxation into mid-bandgap states, or electron−hole recombination. The overall fast decay and the lack of a power dependence can be rationalized as follows. First, a dense manifold of intrinsic mid-bandgap electronic states, associated with several indirect transitions in the visible range,[20] may facilitate rapid relaxation of the initially photoexcited charge carriers into these lower-lying excited states. Second, since the Fe^{3+} defect, common for both γ-Fe_2O_3 and α-Fe_2O_3, has been thought to contribute to poor photoconductivity in polycrystalline as well as single-crystal films,[24,31] a high density of trap states is expected and would make trapping more efficient and push the threshold for observing exciton−exciton annihilation to a higher excitation intensity. Even if the density of trap states is not significantly greater for Fe_2O_3 relative to the other semiconductors described above, trapping could be more efficient simply because of

stronger coupling between the conduction band and trap states or between shallow traps and deep traps. If electrons initially in the conduction band or in shallow traps, which absorb in the 660−850 nm probe range, quickly decay to deep traps or mid-bandgap states with a smaller absorption cross section in the probe region, decay in the transient absorption signal should be observed, and the decay time constants should reflect trapping or relaxation into the mid-bandgap states. The problem with this explanation is the lack of probe wavelength dependence of the observed dynamics, since if trapping or relaxation from the conduction band is the dominant decay mechanism, a spectral blue shift, and thus probe wavelength-dependent decay dynamics, would be expected as the electrons are trapped or relax into lower energy states that are more localized. One possible explanation for the probe wavelength-independent dynamics is that the decays observed are mostly due to nonradiative recombination facilitated by trap states and mid-bandgap states that have no or little absorption in the probe region.

Finally, if the initial transient absorption signal is actually due to electrons in trap states or mid-bandgap states, the trapping process or relaxation from the initial excited state to the mid-bandgap states must be complete within the laser pulse (<150 fs), and the decay dynamics observed then reflect the relaxation of the electrons in these trap or mid-bandgap states. The fact that the decay is very fast and that the fluorescence is very weak suggests that the further decay from these trap or mid-bandgap states is primarily nonradiative. The most likely explanation for the decays in this case is nonradiative electron−hole recombination facilitated by a large number of trap and/or mid-bandgap states.

If trap states play a critical role in the trapping and subsequent recombination processes discussed above, these processes are expected to be sensitive to the surface defects of the particles since many surface traps are caused by surface defects. One might expect then that these processes can be influenced by adsorbates that bind to surface trap sites. However, the adsorbates deoxykenocholic acid and Orange II were found to have no effect on this decay, nor did variations in pH. It is possible that the density of trap states is so great, including internal and interstitial traps not accessible to adsorbates, that trap blocking is difficult to achieve. It is also possible that the trap states are mostly internal rather than surface related. For example, it is well-known that a high density of trap states, due primarily to oxygen vacancies, exists in films of iron oxides.[24,31] However, when doping with transition-metal ions was used to modify the internal lattice and electronic structure of Fe_2O_3 nanoparticles, no change was observed in the electron dynamics either. The dopants used are known to affect the magnetic properties of γ-Fe_2O_3 particles[44−46] and are expected to influence the lattice and electronic structures. The fact that doping has no effect on the electron relaxation dynamics suggests that the dopants did not significantly alter or remove the relevant electronic states responsible for the fast electronic relaxation. This insensitivity of the decay profile to modifications of the surface and to internal dopants suggests that the electron relaxation mechanisms responsible for the triple-exponential profile may be primarily controlled by the intrinsic high density of electronic states of Fe_2O_3 or internal defect-induced trap states.

As shown in Figure 4, γ-Fe_2O_3 and α-Fe_2O_3 have identical transient absorption decay profiles. Since the particles differ in shape and crystal structure, these characteristics do not seem to influence the dynamics of the photoexcited electrons probed in the 660−850 nm range. The electronic structures of γ-Fe_2O_3 and α-Fe_2O_3 are very similar, as shown by their absorption and emission spectra (Figure 2) and calculations.[20] Also, the nature of surface and internal defects to which electrons and holes may trap is likely to be quite similar for the different samples. The commercial sample of γ-Fe_2O_3 had a broad size distribution centered closer to 50 nm average particle size, at least a factor of 10 larger than the γ-Fe_2O_3 sample synthesized in our lab. The fact that transient absorption decay for the commercial sample agrees with the decays observed for the other two samples of much smaller particles suggests that particle size and preparation method do not significantly affect the relaxation pathways. This again seems to suggest that the very fast relaxation is mostly caused by internal defect states or intrinsic mid-bandgap states rather than surface defects.

Conclusion

Photoexcited electrons in spherical γ-Fe_2O_3 and spindle-shaped α-Fe_2O_3 particles exhibit fast power-independent relaxation dynamics. The very fast decay is possibly due to a high density of intrinsic mid-bandgap electronic states, internal defect-induced trap states, and, to a lesser extent, surface defects. It is presently difficult to associate each of the three decays (0.36, 4.2, and 67 ps time constants) to specific processes, since the relaxation processes are all very fast and likely to be interrelated. It is most likely that the decays correspond to electron−hole recombination mediated by intrinsic mid-bandgap states and trap states. The key results are that the overall charge carrier decay for Fe_2O_3 is extremely fast and power-independent and that no measurable transient absorption remains beyond ~100 ps. Since the observed emission is very weak, the decays are clearly mostly nonradiative. The results indicate that visible/near-UV light induced charge separation in Fe_2O_3 nanoparticles is very short-lived. This provides some insight into the poor efficiency of Fe_2O_3 as an electrode material and as a photocatalyst. If photo- or electrogenerated electrons decay rapidly from the conduction band, due either to the intrinsic electronic structure of the material or to a high density of trap states, poor conductivity would be expected, which is what has been previously observed. It remains an interesting and challenging problem to try to develop techniques to influence the properties of Fe_2O_3, such as the electronic structure or density of trap states, so that a longer photoexcited charge carrier lifetime and thereby more efficient charge separation can be achieved.

Acknowledgment. We would like to thank the University of California Energy Institute, the American Chemical Society Petroleum Research Fund, and the University of California at Santa Cruz for funding. D.B.L. gratefully acknowledges an NSF Summer Undergraduate Research Fellowship. We thank Jayasundera Bandara for suggesting the use of Orange II as a surface adsorbate.

References and Notes

(1) Cornell, R. M.; Schwertmann, U. *The Iron Oxides*; VCH: New York, 1996.
(2) Yang, B. L.; Kung, H. H. *J. Catal.* **1982**, *77*, 410.
(3) Leland, J. K.; Bard, A. J. *J. Phys. Chem.* **1987**, *91*, 5076.
(4) Lehman, R. G.; Cheng, H. H.; Harsh, J. B. *Soil Sci. Soc. Am. J.* **1987**, *51*, 352.
(5) Faust, B. C.; Hoffmann, M. R.; Bahnemann, D. W. *J. Phys. Chem.* **1989**, *93*, 6371.
(6) Liaw, B. J.; Cheng, D. S.; Yang, B. L. *J. Catal.* **1989**, *118*, 312.
(7) Chatterjee, S.; Sarkar, S.; Bhattacharyya, S. N. *J. Photochem. Photobiol. A: Chem.* **1993**, *72*, 183.
(8) Pulgarin, C.; Kiwi, J. *Langmuir* **1995**, *11*, 519.
(9) Kang, Y. S.; Risbud, S.; Rabolt, J. F.; Stroeve, P. *Chem. Mater.* **1996**, *8*, 2209.

(10) Vassiliou, J. K.; Mehrotra, V.; Russell, M. W.; Giannelis, E. P. *J. Appl. Phys.* **1993**, *73*, 5109.
(11) Ziolo, R. F.; Giannelis, E. P.; Weinstein, B. A.; O'Horo, M. P.; Ganguly, B. N.; Mehrotra, V.; Russell, M. W.; Huffman, D. R. *Science* **1992**, *257*, 219.
(12) Chang, W. D.; Chin, T. S. *IEEE Trans. Magn.* **1996**, *32*, 3620.
(13) Ozaki, M.; Matijevic, E. *J. Colloid Interface Sci.* **1985**, *107*, 199.
(14) del Monte, F.; Morales, M. P.; Levy, D.; Fernandez, A.; Ocaña, M.; Roig, A.; Molins, E.; O'Grady, K.; Serna, C. J. *Langmuir* **1997**, *13*, 3627.
(15) Bacri, J.-C.; Perzynski, R.; Salin, D.; Cabuil, V.; Massart, R. *J. Magn. Magn. Mater.* **1986**, *62*, 36.
(16) Zhang, L.; Papaefthymiou, G. C.; Ying, J. Y. *J. Appl. Phys.* **1997**, *81*, 6892.
(17) Parker, F. T.; Foster, M. W.; Margulies, D. T.; Berkowitz, A. E. *Phys. Rev. B* **1993**, *47*, 7885.
(18) Tronc, E.; Prené, P.; Jolivet, J. P.; Giorani, D.; Testa, A. M.; Cherkaoui, R.; Noguès, M.; Dormann, J. L. *Nanostruct. Mater.* **1995**, *6*, 945.
(19) Vollath, D.; Szabó, D. V.; Taylor, R. D.; Willis, J. O.; Sickafus, K. E. *Nanostruct. Mater.* **1995**, *6*, 941.
(20) Sherman, D. M.; Waite, T. D. *Am. Mineral.* **1985**, *70*, 1262.
(21) Quinn, R. K.; Nasby, R. B.; Braughman, R. J. *Mater. Res. Bull.* **1976**, *11*, 1011.
(22) Yeh, L.-S.; Hackerman, N. *J. Electrochem. Soc.* **1977**, *124*, 833.
(23) Hardee, K. L.; Bard, A. J. *J. Electrochem. Soc.* **1978**, *123*, 1024.
(24) Dare-Edwards, M. P.; Goodenough, J. B.; Hamnett, A.; Trevellick, P. R. *J. Chem. Soc., Faraday Trans. 1* **1983**, *79*, 2027.
(25) Somorjai, G. A.; Salmeron, M. In *Homogeneous and Heterogeneous Photocatalysis*; Pelizzetti, E., Serpone, N., Eds.; D. Reidel: Boston, 1986; p 445.
(26) Kiwi, J.; Grätzel, M. *J. Chem. Soc., Faraday Trans. 1* **1987**, *83*, 1101.
(27) Anderman, M.; Kennedy, J. H. In *Semiconductor Electrodes*; Finklea, H. O., Ed.; Elsevier: New York, 1988; p 147.
(28) Cai, S.; Jiang, D.; Tong, R.; Jin, S.; Zhang, J.; Fujishima, A. *Electrochim. Acta* **1991**, *36*, 1585.
(29) Gurunathan, K.; Maruthamuthu, P. *Int. J. Hydrogen Energy* **1995**, *20*, 287.
(30) Zhang, Z.; Boxall, C.; Kelsall, G. H. *Colloids Surf., A* **1993**, *73*, 145.
(31) Leygraf, C.; Hendewerk, M.; Somorjai, G. *J. Solid State Chem.* **1983**, *48*, 357.
(32) Roberti, T. W.; Cherepy, N. J.; Zhang, J. Z. *J. Chem. Phys.*, in press.
(33) Colombo, D. P.; Roussel, K. A.; Saeh, J.; Skinner, D. E.; Cavaleri, J. J.; Bowman, R. M. *Chem. Phys. Lett.* **1995**, *232*, 207.
(34) Matijevic, E. *Faraday Discuss.* **1991**, *92*, 229.
(35) Schwertmann, U.; Cornell, R. M. *Iron Oxides in the Laboratory*; VCH: New York, 1991.
(36) Sugimoto, T.; Muramatsu, A. *J. Colloid Interface Sci.* **1996**, *184*, 626.
(37) Zhang, J. Z.; O'Neil, R. H.; Roberti, T. W. *J. Phys. Chem.* **1994**, *98*, 3859.
(38) Kay, A.; Grätzel, M. *J. Phys. Chem.* **1993**, *97*, 6272.
(39) Vinodgopal, K.; Kamat, P. V. *J. Photochem. Photobiol. A: Chem.* **1994**, *83*, 141.
(40) Bandara, J.; Morrison, C.; Kiwi, J.; Pulgarin, C.; Peringer, P. *J. Photochem. Photobiol. A: Chem.* **1996**, *99*, 57.
(41) Cavaleri, J. J.; Skinner, D. E.; Colombo, D. P.; Bowman, R. M. *J. Chem. Phys.* **1995**, *103*, 5378.
(42) Dimitrijevic, N. M.; Savic, D.; Micic, O. I.; Nozik, A. J. *J. Phys. Chem.* **1984**, *88*, 4278.
(43) (a) Brelle, M.; Zhang, J. Z. *J. Chem. Phys.*, in press. (b) Zhang, J. Z. *Acc. Chem. Res.* **1997**, *30*, 423.
(44) Kuo, P. C.; Chen, J. A.; Pan, C. W. *J. Mater. Sci.* **1993**, *28*, 817.
(45) da Silva, M. F.; Figueiredo Neto, A. M. *Phys. Rev. E* **1993**, *48*, 4483.
(46) Lin, C. H.; Kuo, P. C.; Chen, J. A.; Yao, Y. D. *IEEE Trans. Magn.* **1994**, *30*, 4104.